Electronic Supplementary Information

Halogen-engineered metal-organic frameworks enable high-performance electrochemical glucose sensing

Le Wang[a]†, Yong-Shuang Li[a]†, Meidi Wang[a,b], Zhuo-Hao Wu[a,b], Ya-Pan Wu[a,b], Yu Cao[c], Xue-Qian Wu[a,b], Dong-Sheng Li[a,b]**

[a]College of Materials and Chemical Engineering, Key Laboratory of Inorganic Nonmetallic Crystalline and Energy Conversion Materials, China Three Gorges University, Yichang, Hubei, 443002, P.R. China

[b]Hubei Three Gorges Laboratory, Yichang, Hubei, 443007, P. R. China

[c]School of Chemical Engineering and Technology, Tianjin University, Tianjin 300072, P. R. China

†These authors contributed equally to this work.

Materials and Experiments

Materials. Nickel acetate tetrahydrate ($Ni(CH_3COO)_2 \cdot 4H_2O$), Nickel perchlorate hexahydrate ($Ni(ClO_4)_2 \cdot 6H_2O$), 3,4,5,6-tetrafluorophthalic acid (H_2F_4ph), 3,4,5,6-tetrachlorophthalic acid (H_2Cl_4ph), 3,4,5,6-tetrabromophthalic acid (H_2Br_4ph), 4,4'-bipyridine (4,4′-bipy), potassium hydroxide (KOH), glucose, sodium chloride (NaCl), urea (UR), fructose (Fru), L-Ascorbic acid (AA), lactose (Lac), dopamine hydrochloride (DA), anhydrous ethanol, anhydrous methanol were purchased from Shanghai Macklin Biochemical Co., Ltd and used without further purification. The glassy carbon electrode (GCE) was obtained from Tianjin Aida Hengsheng Technology Development Co., LTD and used as the working electrode. Certified fetal bovine serum was purchased from Shanghai XP Biomed Ltd. Deionized water with a specific resistance of 18.25 MΩ were used throughout the experiments in this work.

Synthesis of CTGU-37-Cl. 0.04 mmol $Ni(CH_3COO)_2 \cdot 4H_2O$ (9.9536 mg), 0.04 mmol 3,4,5,6-tetrachlorophthalic acid (H_2Cl_4ph, 12.1546 mg), 0.04 mmol 4,4'-bipyridine (4,4′-bipy, 6.2472 mg) and 6 mL deionized water were added into an ampoules (10mL). Next 0.4 mL 0.1M KOH solution was added into the above mixture to get a cloudy

dispersion. The sealed ampoules was transferred to a preheated oven and holding at 120 °C for 72 hours under static conditions. After the reaction, the light green precipitates were cooled to room temperature spontaneously, and subsequently washed three times with deionized water as well as anhydrous ethanol. The washed powders were activated with anhydrous methanol and dried at 60 ℃ under vacuum for 12 h to get light green lumpy crystals.

Yield of product: 91.41% (based on H_2Cl_4ph)

Chemical formula: $C_{18}H_{12}Cl_4NiN_2O_6$ (Mr=552.69)

Elemental analysis calculation (%): C, 39.08; H, 2.17; Cl, 25.69; N, 5.06; Ni, 10.61; O, 17.36.

FT-IR (KBr, cm^{-1}): 3438.51 (s), 2925.53 (w), 1602.58 (s), 1425.16 (w), 1398.16 (w)1344.16 (m), 1220.74 (w), 1132.03 (m), 917.97 (w), 813.83 (m), 626.76 (w).

X-ray crystallography. Diffraction data for CTGU-37-Cl was collected on an XtaLAB PRO MM003 (Cu) using graphite monochromated Cu Kα radiation (λ=1.54184 Å) with the φ/ω scan technique. The crystal structures were decoded by intrinsic phasing methods and refined by the full-matrix least-squares methods on F^2 using Olex2-1.5 and SHELXTL. The non-hydrogen atoms were refined anisotropically. The details of crystal data and structure refinement are given in Table 1.

Table S1. Crystal data and structure refinement parameters of CTGU-37-Cl.

Ni-MOF	Cl-MOF
Empirical formula	$C_{18}H_{12}Cl_4NiN_2O_6$
Formula weight	552.69
Crystal system	orthorhombic
Space group	Pccn
a (Å)	7.43760(10)
b (Å)	11.9779(3)
c (Å)	22.9882(5)
α(°)	90
β(°)	90
γ(°)	90

Volume (Å^3)	2047.95(7)
Z	8
ρ_{calc} (g·cm^{-3})	1.793
F(000)	1112.0
Reflections collected	5667
Independent data	2015
Rint	0.0560
Goodness-of-fit on F^2	1.063
R_1 [I >2σ(I)]	0.0441
wR_2 [I >2σ(I)]	0.1111
R_1 (all data)	0.0556
wR_2 (all data)	0.1163

[a]$R=\Sigma|F_0||F_C|/\Sigma|F_0|$, [b]$wR_2=[\Sigma[w(F_0^2-FC^2)^2]/\Sigma[(F_0^2)^2]]^{1/2}$

Characterization. Powder X-ray diffraction (PXRD) pattern were obtained on a Rigaku Ultima IV diffractometer (CuKα radiation, λ=1.5406 Å) with a scan speed of 8 °/min and a step size of 0.02° at 2θ. X-ray photoelectron spectroscopy (XPS) analysis was conducted on an ESCALAB MKLL X-ray photoelectron spectrometer. Scanning electron microscopy (SEM) images were obtained on a JEOL JSM 6700F instruments. The two-dimensional morphology and and elemental mapping analysis of CTGU-37 were characterized by transmission electron microscopy (TEM)on a JEOL JEM 2010F instrument at an acceleration voltage of 200 kV. Fourier transform infrared (FT-IR) spectra were recorded on a Nexus 670 spectrophotometer equipped with KBr pellets. Thermogravimetric analysis (TGA) was carried out with a TGA-50 thermogravimetric analyzer with a heating rate of 10 °C/min under air atmosphere. Electrochemical measurements were conducted at ambient conditions using a CHI660E electrochemical analyzer.

Electrochemical tests. Electrochemical glucose sensing were performed in a standard three-electrode system using a CHI660E electrochemical workstation (Shanghai Chenhua Instruments Co., Ltd.) at ambient temperature. Cyclic voltammetry (CV) and

constant potential chronoamperometry (i-t) curve studies were carried out to evaluate the sensing performance of CTGU-37-F, Cl, Br. A MOF-modified glassy carbon electrode (GCE) was used as the working electrode. A platinum wire and Hg/HgO were utilized as the counter electrode as well as the reference electrode, respectively.

Preparation of the working electrode: 4 mg of CTGU-37 was ground in an agate mortar for 10 min. The finely-divided powders were added into 2 mL of mixed solvent (0.5 mL ethanol, 1.3 mL H_2O, 0.2 mL 0.5% Nafion aqueous solution). The above mentioned dispersion was undergone ultrasonic treatment for 30 min to get a homogeneously dispersed slurry, 5 μL of such slurry was pipetted and dropwise added on the surface of the polished GCE. The working electrode was obtained after dried at room temperature.

Electrochemical impedance spectroscopy (EIS) was tested in the similar protocol with electrochemical glucose sensing performance. It should be noted that CTGU-37-F, -Cl, -Br are tested at 0.5 V potential with the low frequency of 0.1 Hz, high frequency of 10^5 Hz and amplitude of 0.005 V.

Density functional theory (DFT) calculations. Material Studio software was used for the DFT calculations, which were performed using Dmol3 program[1,2]. Generalized gradient approximation with Perdew-Burke-Ernzerhof (GGA-PBE) function was used for the exchange-correlation[3]. For the simulation of non-bonded interlayer interaction energy, two adjacent layers were located according to the crystal parameter. Then the whole system was optimized by the Forcite module to reach a thermodynamically equilibrium state with the minimum energy. The SCF convergence for each electronic energy was set as 1.0×10^{-6} Ha. The convergence tolerances of energy, force and displacement were set at 1×10^{-5} Ha, 0.002 Ha $Å^{-1}$, and 0.005 Å, respectively. The binding energy was calculated in accordance with the following equations:

$$\Delta E = E_{system} - 2\times E_{monolayer}$$

where E_{system} is the energy of double layer system and $E_{monolayer}$ is the energy of monolayer of MOF.

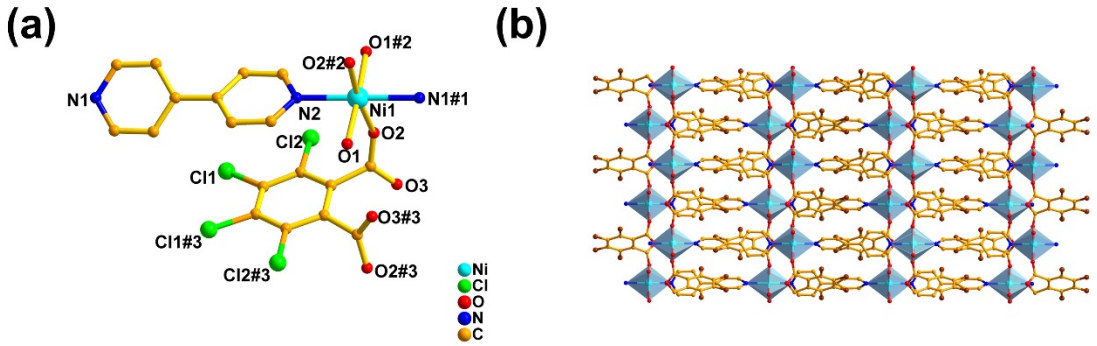

Figure S1. (a) Coordination environments of Ni^{2+} in CTGU-37-Cl. Symmetry codes: #1: 3/2-X, 1/2-Y, Z; #2: X, 1/2-Y, -1/2+Z; #3: 1/2-X, 1/2-Y, Z; #4: X, 1/2-Y, 1/2+Z. (b) View of 3D frameworks of CTGU-37-Cl.

Table S2. Selected bond lengths (Å) for CTGU-37-Cl

Bond	lengths (Å)	Bond	lengths (Å)
Ni1-O2	2.0674(18)	Ni1-N2	2.180(3)
Ni1-O2#1	2.0674(18)	Ni1-N1#2	2.185(3)
Ni1-O1#1	2.042(2)	Cl2-C9	1.723(3)
Ni1-O1	2.042(2)	Cl1-C10	1.723(3)

Symmetry codes: #1: 2/3-X, 1/2-Y, +Z; #2: +X, 1/2-Y, -1/2+Z; #3: 1/2-X, 1/2-Y, +Z.

Table S3. Selected bond angles (°) for CTGU-37-Cl

Bond	Angels (deg.)	Bond	Angels (deg.)
O2-Ni1-O2#1	172.75(11)	O1#1-Ni1-N2	88.74(5)
O2-Ni1-N2	93.63(5)	O1#1-Ni1-N1#2	91.26(5)
O2#1-Ni1-N2	93.63(5)	N2-Ni1-N1#2	180.0
O2#1-Ni1-N1#2	86.37(5)	C7-O2-Ni1	144.1(2)
O2-Ni1-N1#2	86.37(5)	C6#1-N2-Ni1	121.68(16)
O1#1-Ni1-O2	86.24(8)	C6-N2-Ni1	121.68(16)
O1-Ni1-O2	93.92(8)	C1-N1-Ni1#3	121.85(16)
O1-Ni1-O2#1	86.24(8)	C1#1-N1-Ni1#3	121.85(16)
O1#1-Ni1-O2#1	93.92(8)	C10#4-C10-Cl1	120.42(11)
O1#1-Ni1-O1	177.47(11)	C9-C10-Cl1	119.9(2)
O1-Ni1-N2	88.73(5)	C8-C9-Cl2	118.9(2)
C10-C9-Cl2	120.7(2)		

Symmetry codes: #1:3/2-X, 1/2-Y, +Z; #2: +X, 1/2-Y, -1/2+Z; #3: +X, 1/2-Y, 1/2+Z; #4: 1/2-X, 1/2-Y, +Z.

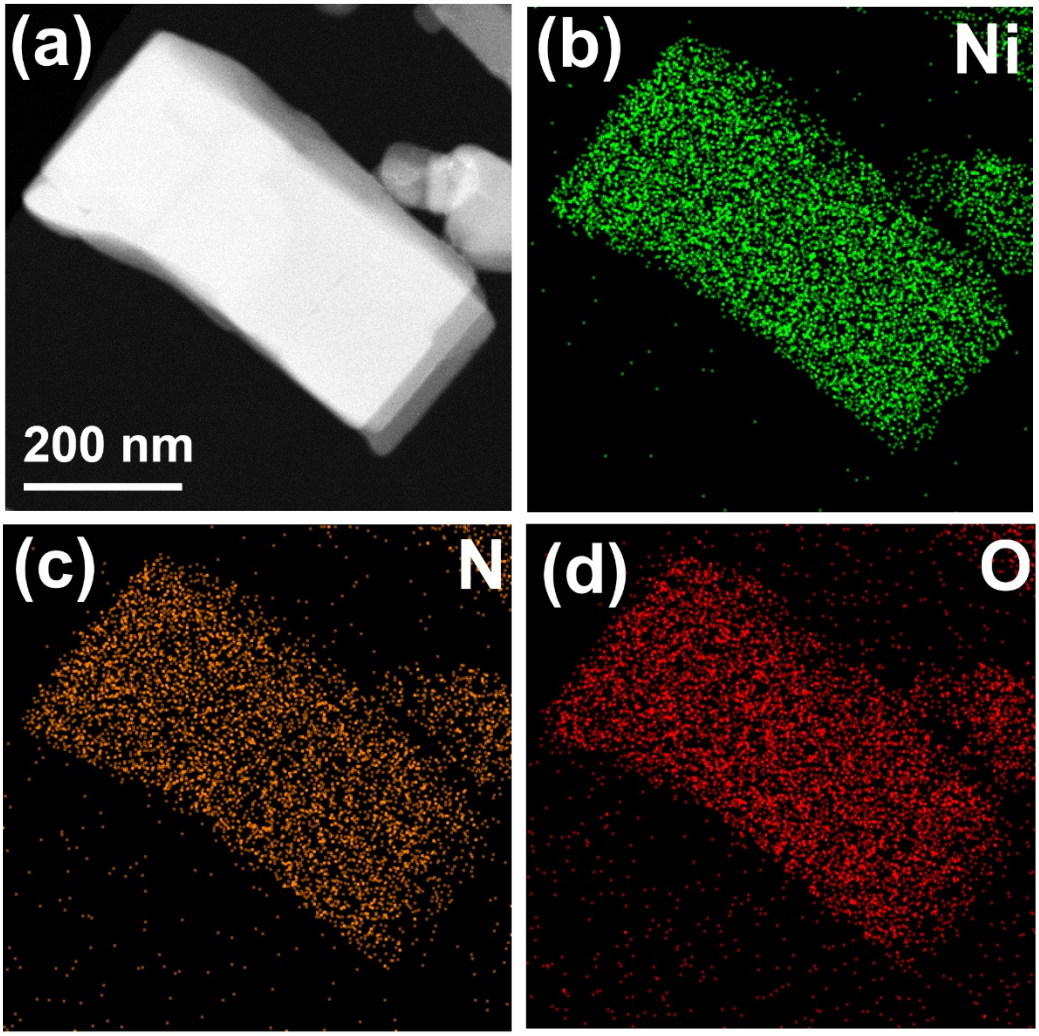

Figure S2. (a) TEM image of CTGU-37-F and the corresponding elemental mapping images of (b) Ni, (c) N, (d) O.

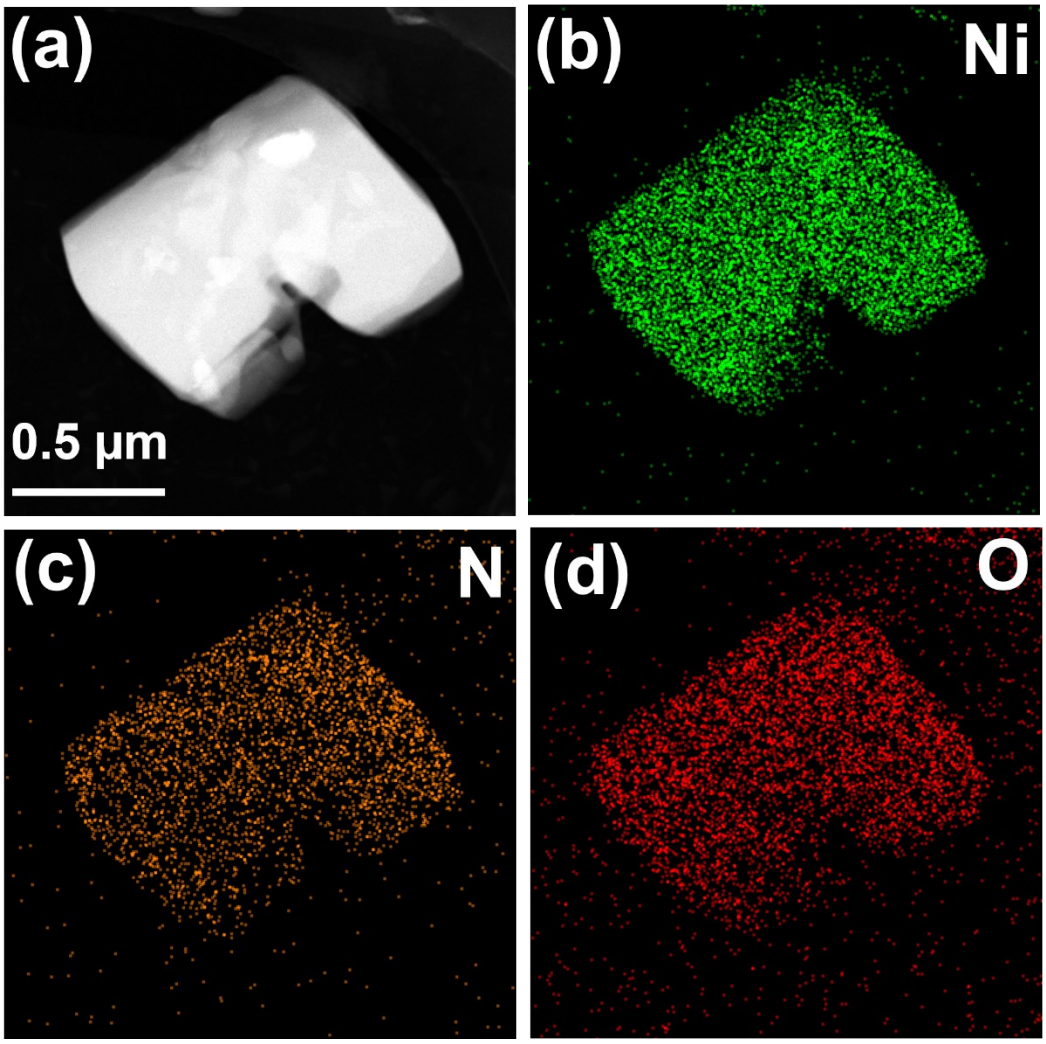

Figure S3. (a) TEM image of CTGU-37-Cl and the corresponding elemental mapping images of (b) Ni, (c) N, (d) O.

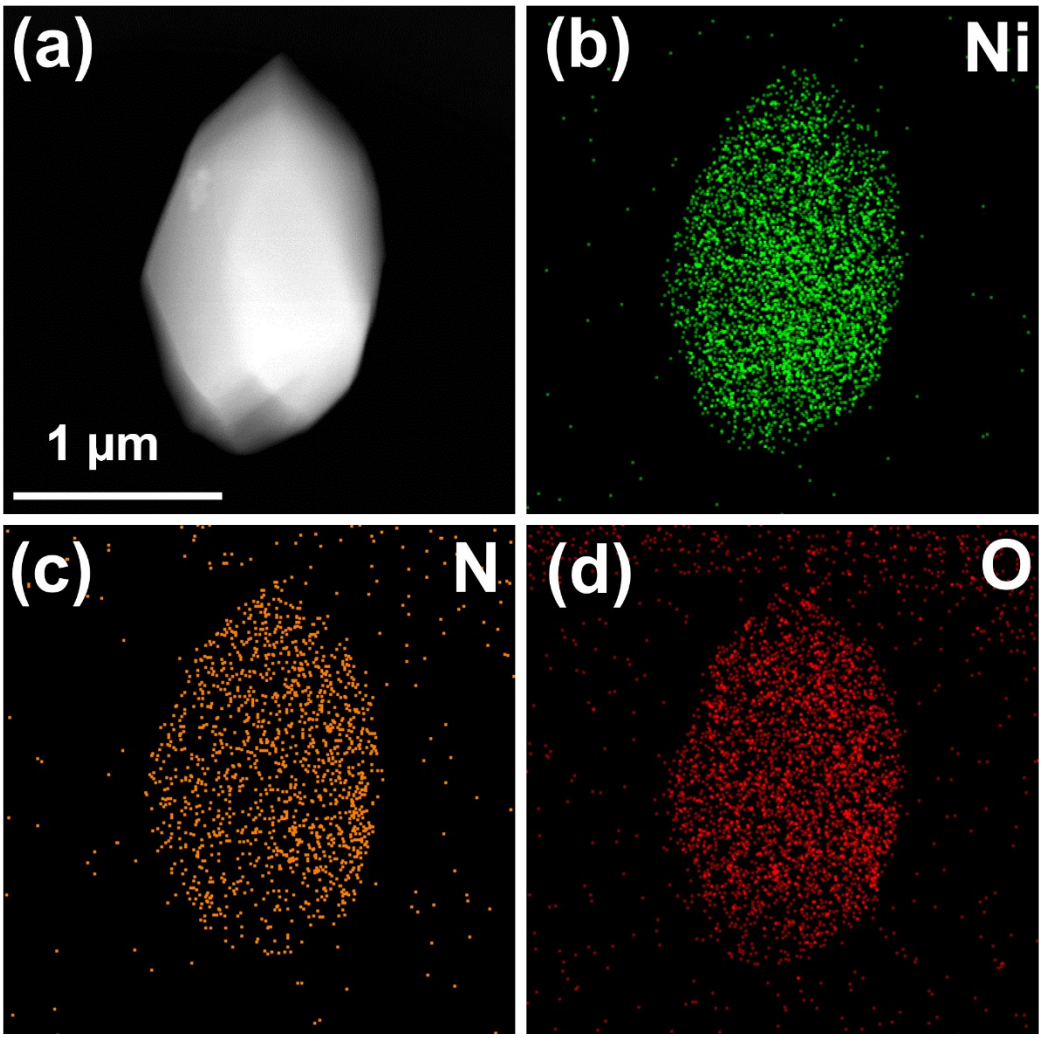

Figure S4. (a) TEM image of CTGU-37-Br and the corresponding elemental mapping images of (b) Ni, (c) N, (d) O.

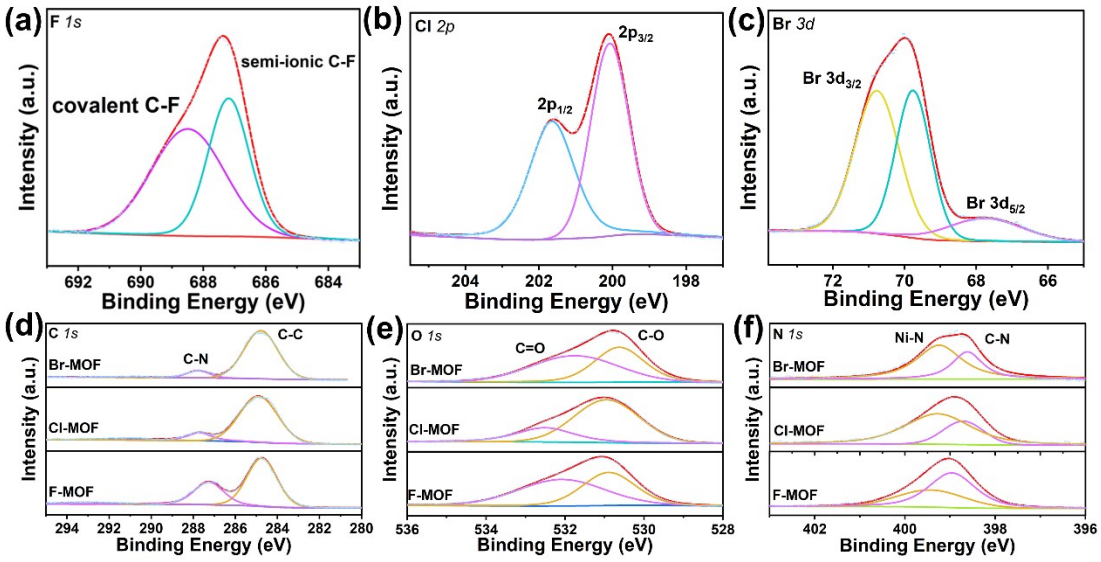

Figure S5. (a) High-resolution XPS spectrum of F *1s* in CTGU-37-F. (b) High-resolution XPS spectrum of Cl *2p* in CTGU-37-Cl. (c) High-resolution XPS spectrum of Br *3d* in CTGU-37-Br. (d) C *1s* spectra of CTGU-37-F, -Cl, -Br, (e) O *1s* spectra of CTGU-37-F, -Cl, -Br, (f) N *1s* spectra of CTGU-37-F, -Cl, -Br.

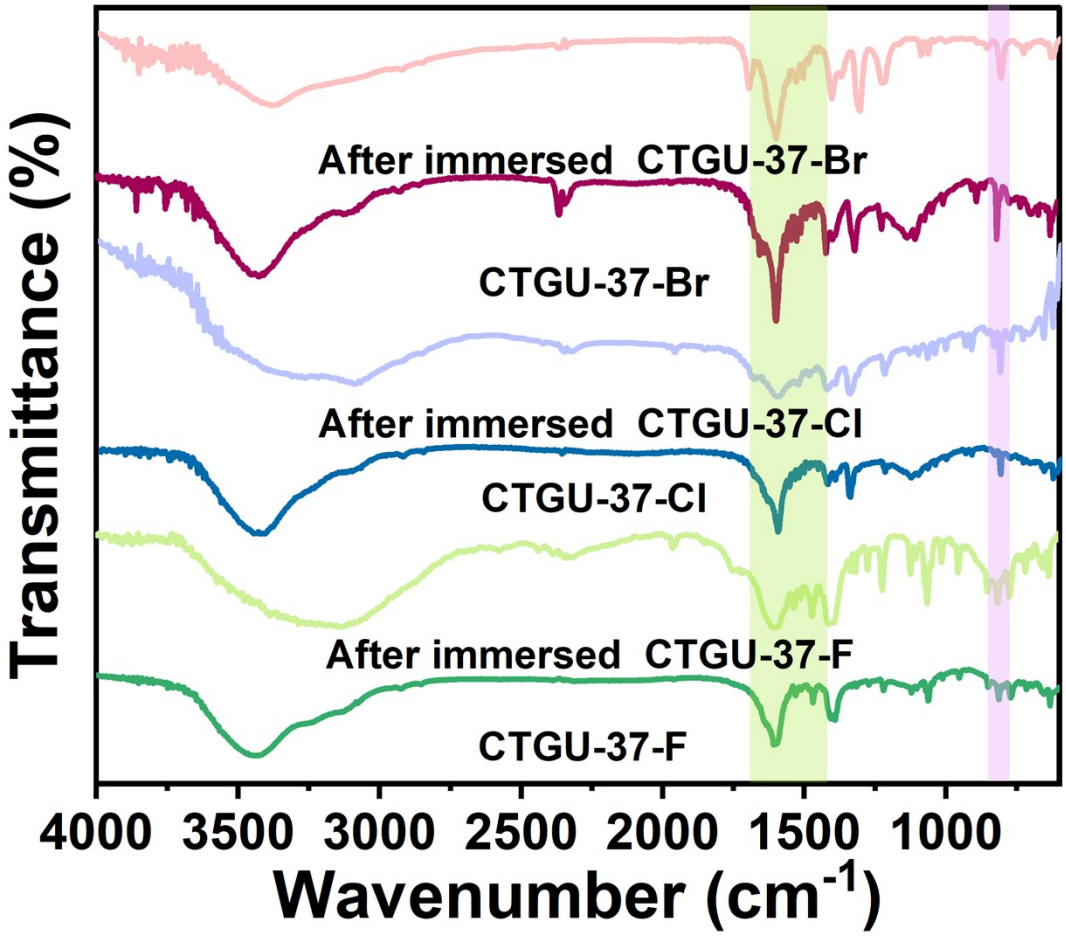

Figure S6. (a) FT-IR spectra of as-synthesized and after immersed (0.1 M NaOH for 24h) CTGU-37-F, -Cl, -Br.

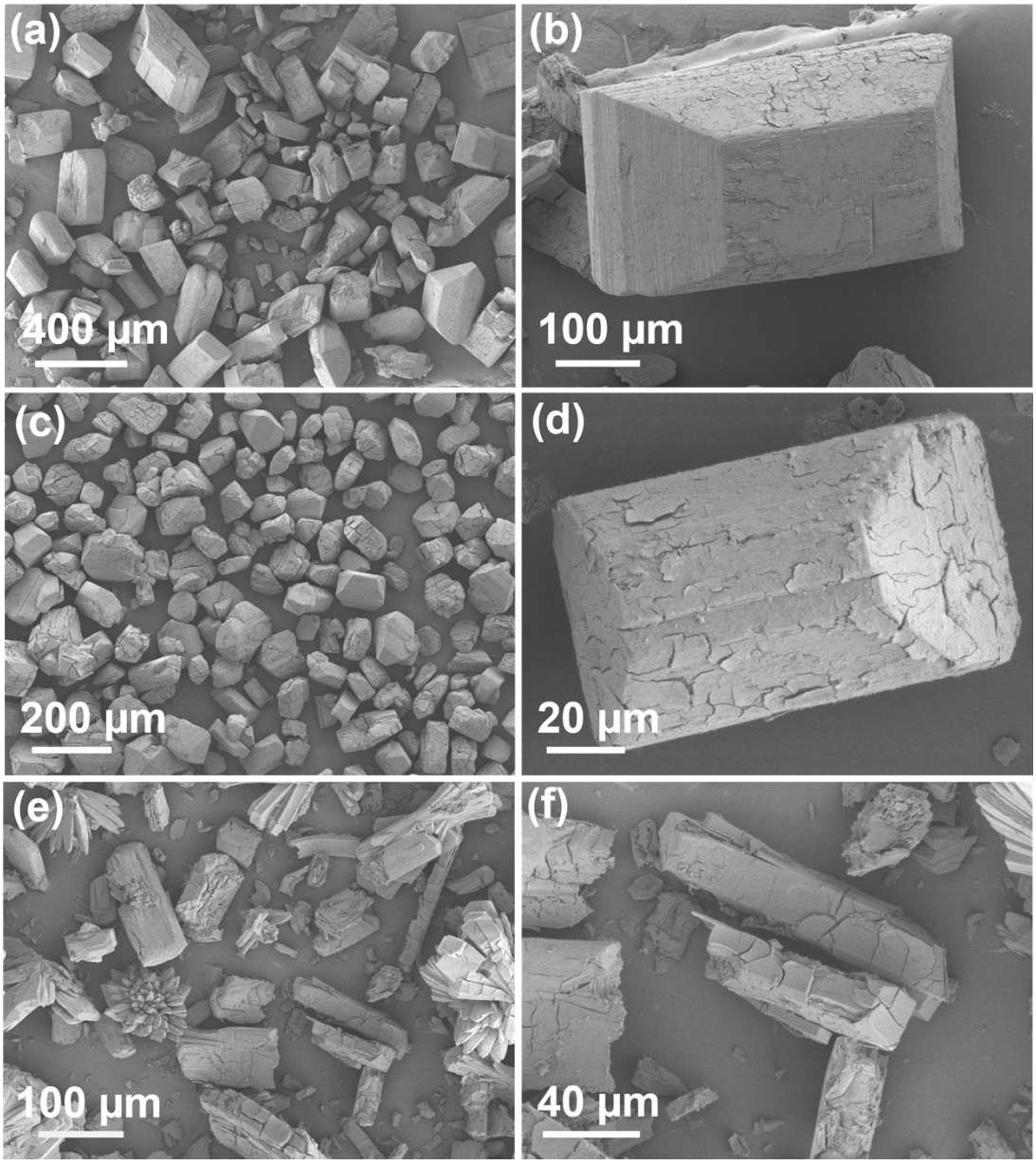

Figure S7.SEM images of (a, b) CTGU-37-F, (c, d) CTGU-37-Cl, (e, f) CTGU-37-Br after immersed (0.1 M NaOH for 24h).

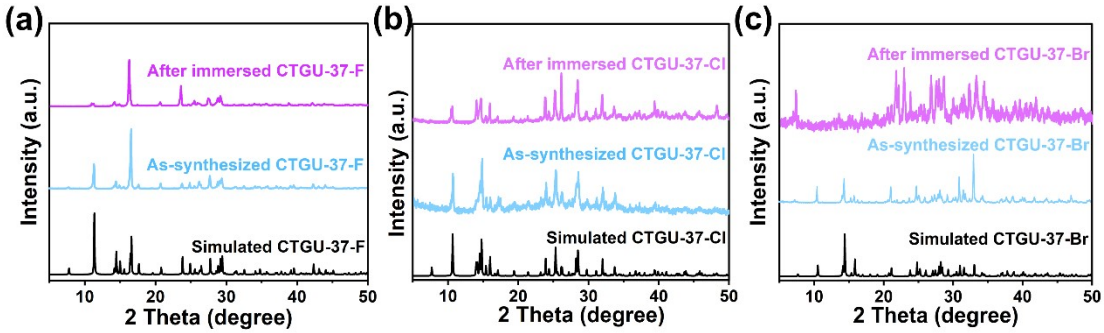

Figure S8. PXRD patterns of simulated, as-synthesized and after immersed (0.1 M NaOH for 24h) (a) CTGU-37-F, (b) CTGU-37-Cl and (c) CTGU-37-Br.

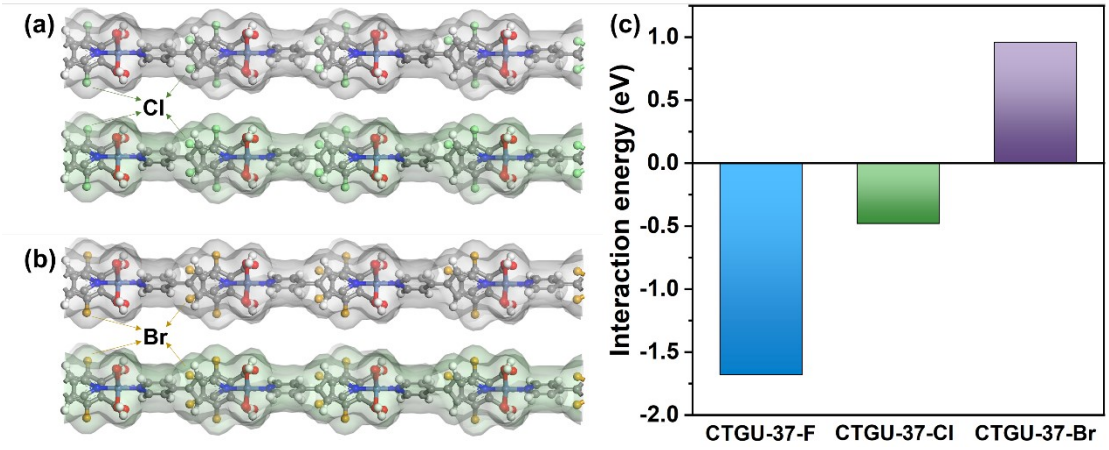

Figure S9. Theoretical calculation study of interlayer interaction of (a) CTGU-37-Cl, and (b) CTGU-37-Br. (c) Calculated binding energy of CTGU-37-F, -Cl, -Br.

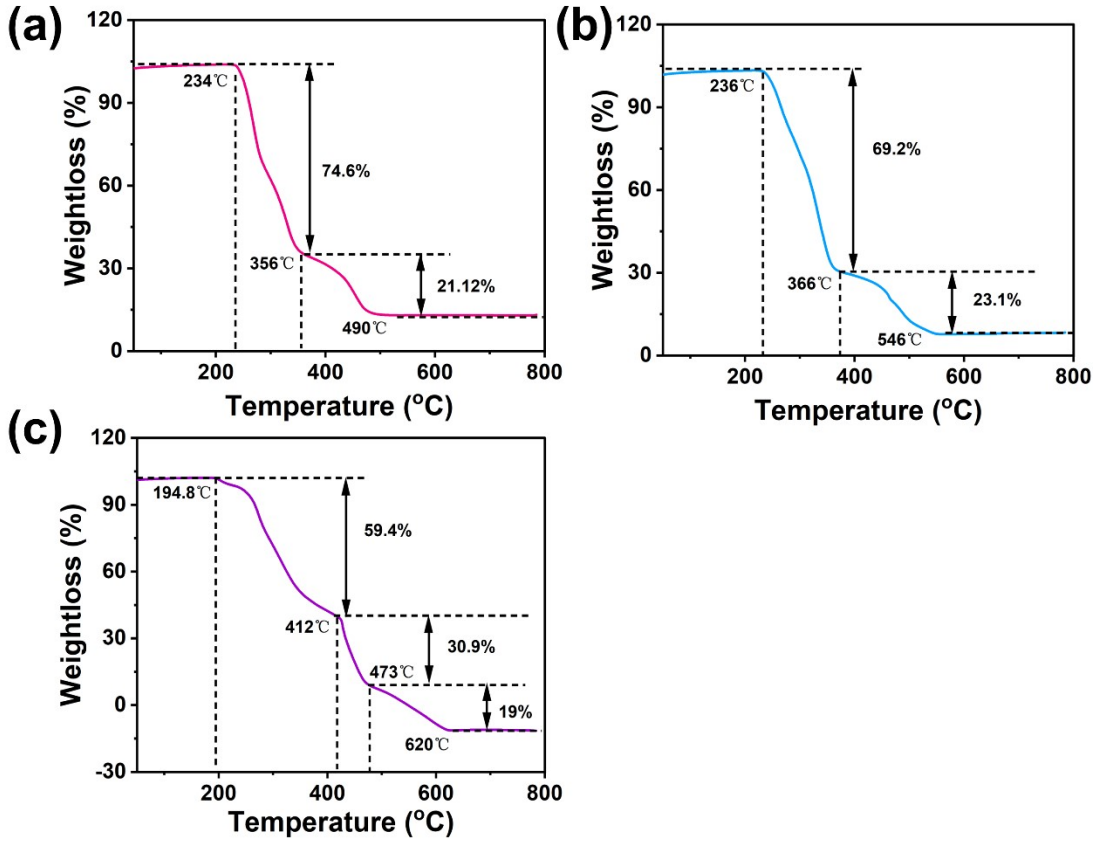

Figure S10. TGA curves of (a) CTGU-37-F, (b) CTGU-37-Cl and (c) CTGU-37-Br.

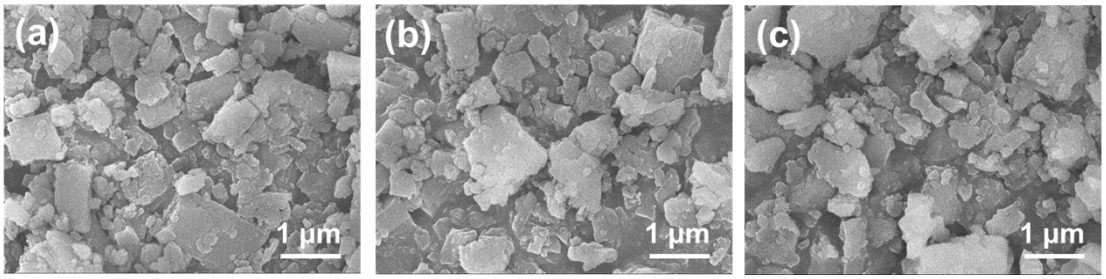

Figure S11. SEM images of (a) CTGU-37-F, (b) CTGU-37-Cl and (c) CTGU-37-Br after the grinding and ultrasonic treatments.

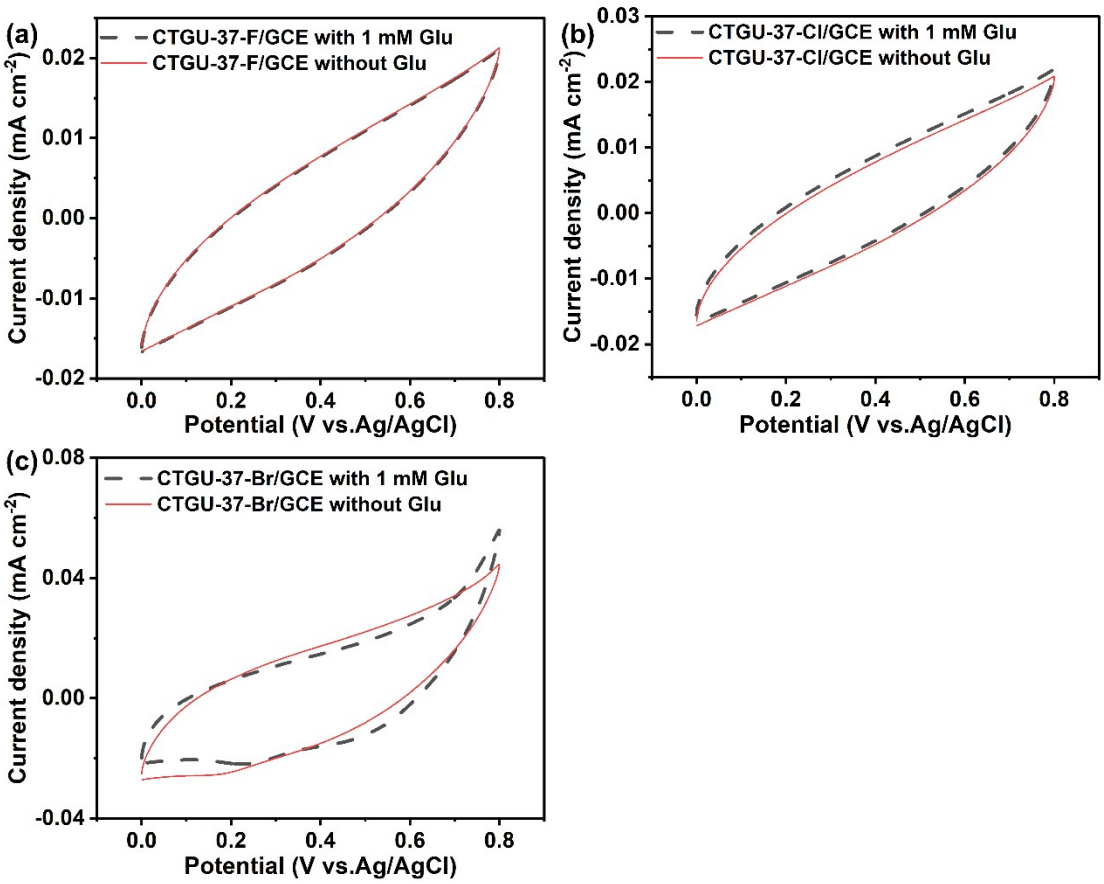

Figure S12. CV curves of (a) CTGU-37-F, (b) CTGU-37-Cl and (c) CTGu-37-Br in the solutions at pH=7.

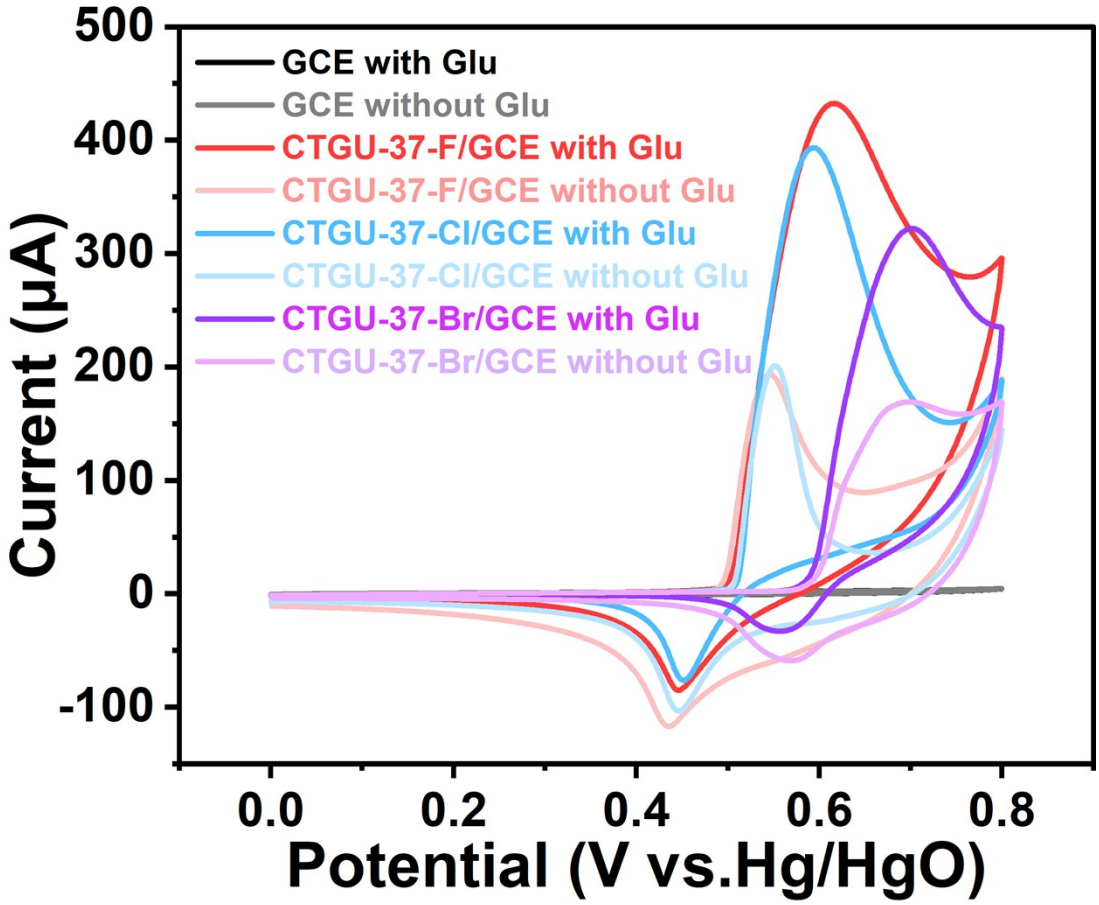

Figure S13. CV curves of CTGU-37-F. -Cl, -Br in 0.1 M NaOH solution in the presence and absence of 1 mM glucose (scan rate: 50 mV s^{-1}).

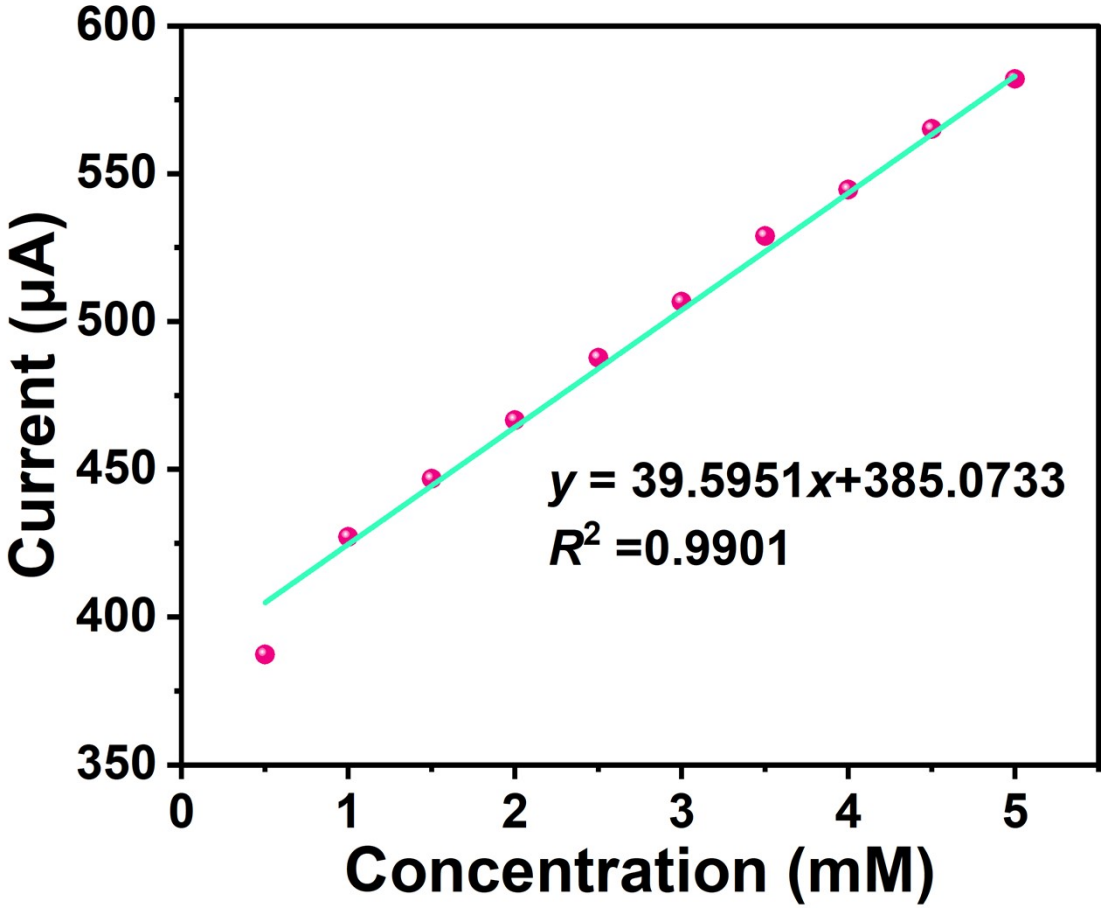

Figure S14. The linear fitting of peak currents with different glucose concentrations of CTGU-37-F.

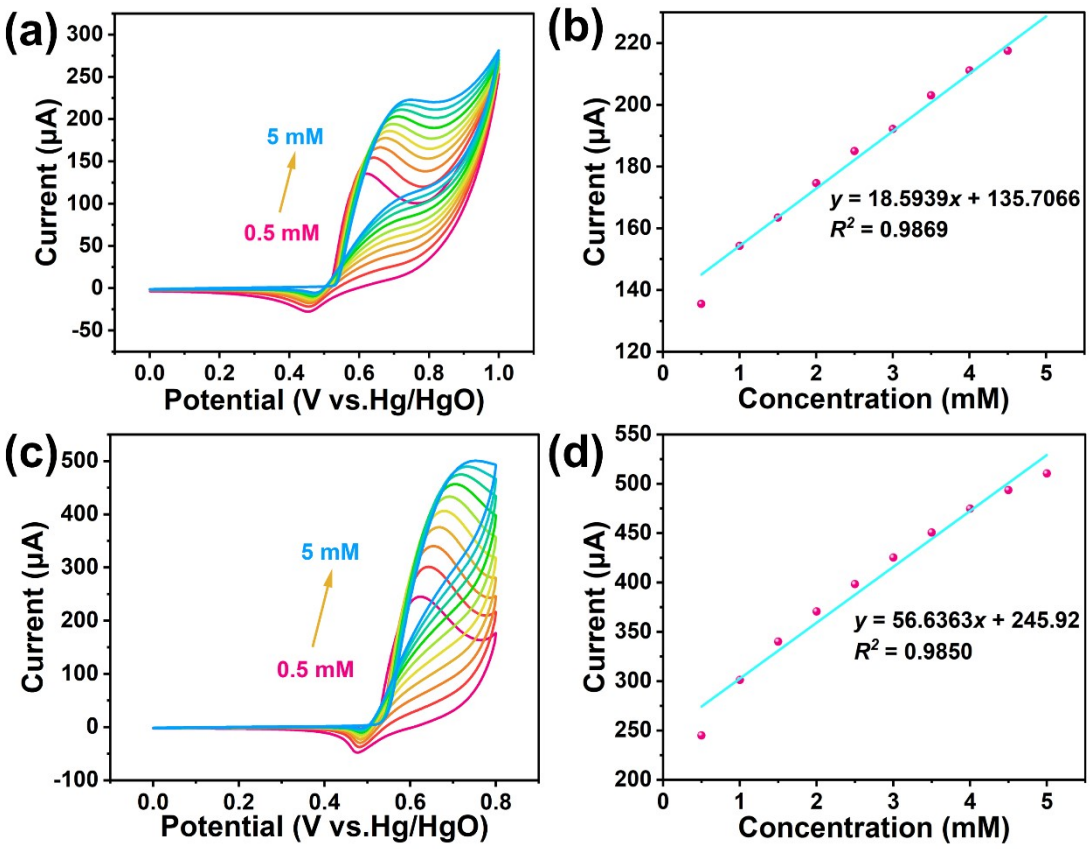

Figure S15. CV curves of (a) CTGU-37-Cl and (c) CTGU-37-Br in 0.1 M NaOH solution with different glucose concentrations (0.5-5 mM, scan rate: 50 mV s^{-1}). (b, d) The corresponding linear fitting of peak currents with different glucose concentrations.

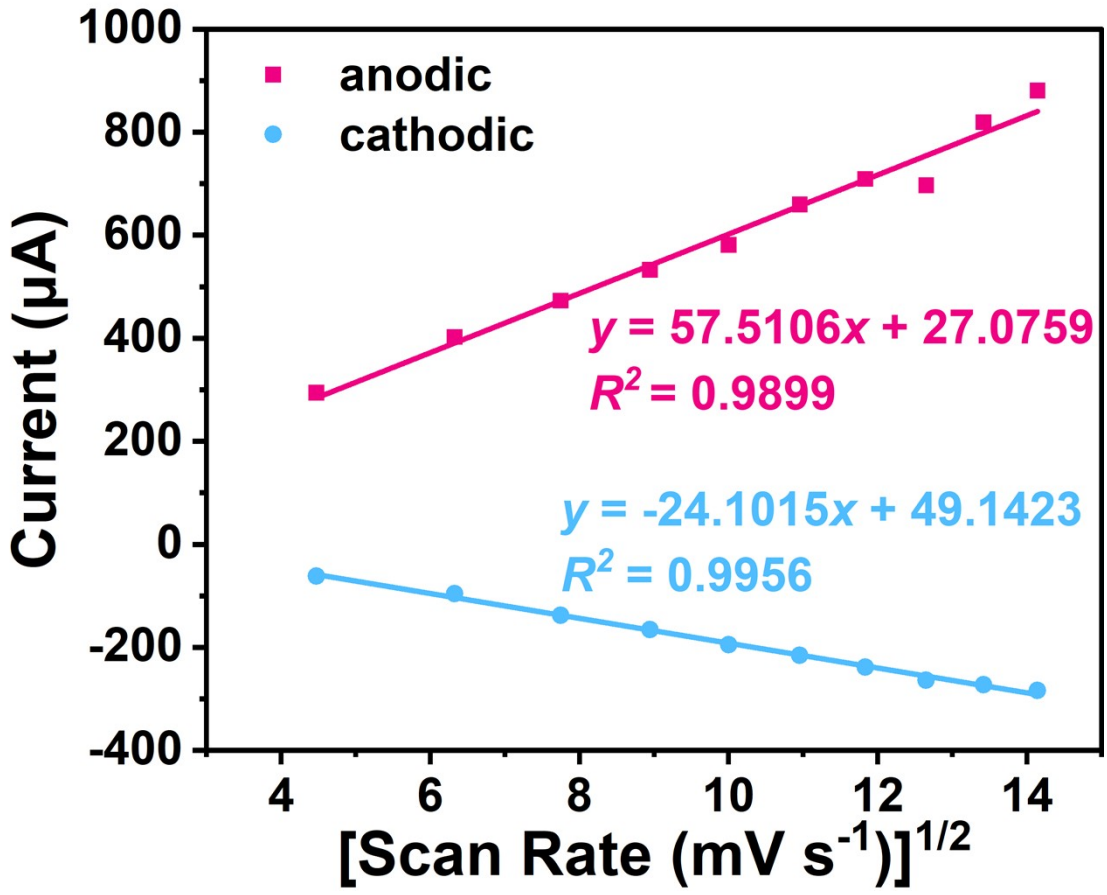

Figure S16. The linear fitting of anodic and cathodic peak current with sqrt scan rate for CTGU-37-F.

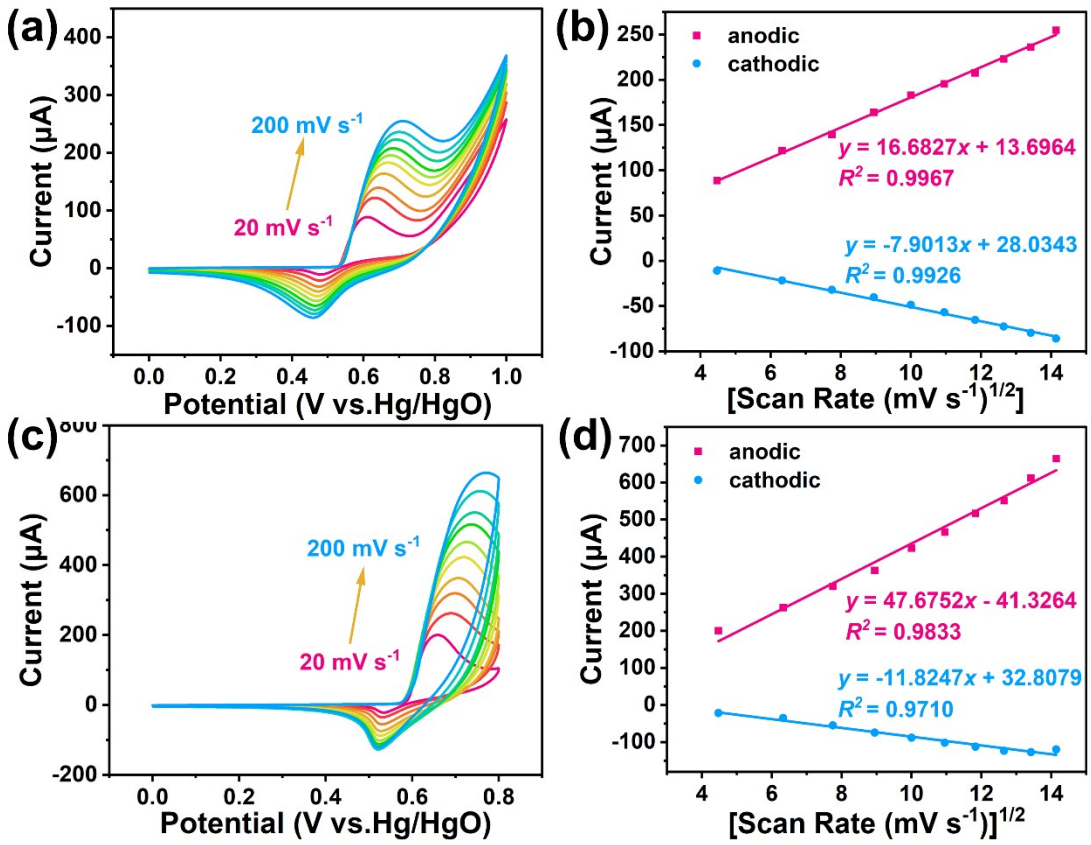

Figure S17. CV curves of (a) CTGU-37-Cl and (c) CTGU-37-Br at scan rates from 20-200 mV s^{-1} in 0.1 M NaOH solution with 1 mM glucose. (b, d) The corresponding linear fitting of anodic and cathodic peak current with sqrt scan rate.

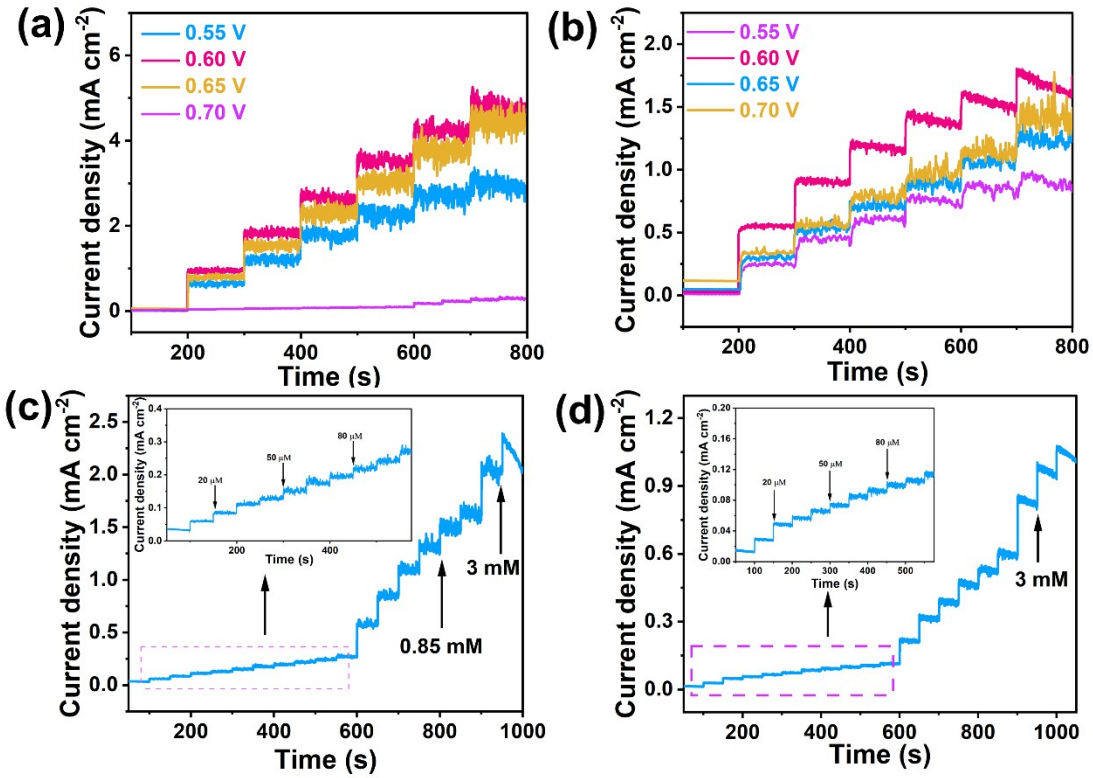

Figure S18. Amperometric response of (a) CTGU-37-Cl and (b) CTGU-37-Br at different potentials (0.55-0.70 V). Amperometric responses of (c) CTGU-37-Cl and (d) CTGU-37-Br at 0.60 V to the continual addition of glucose.

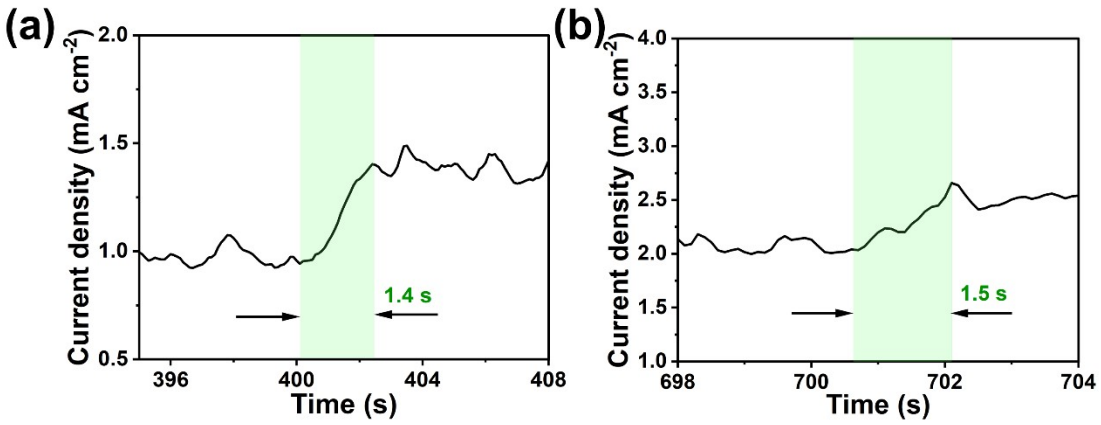

Figure S19. Enlarged view of amperometric response curve for (a) CTGU-37-Cl and (b) CTGU-37-Br.

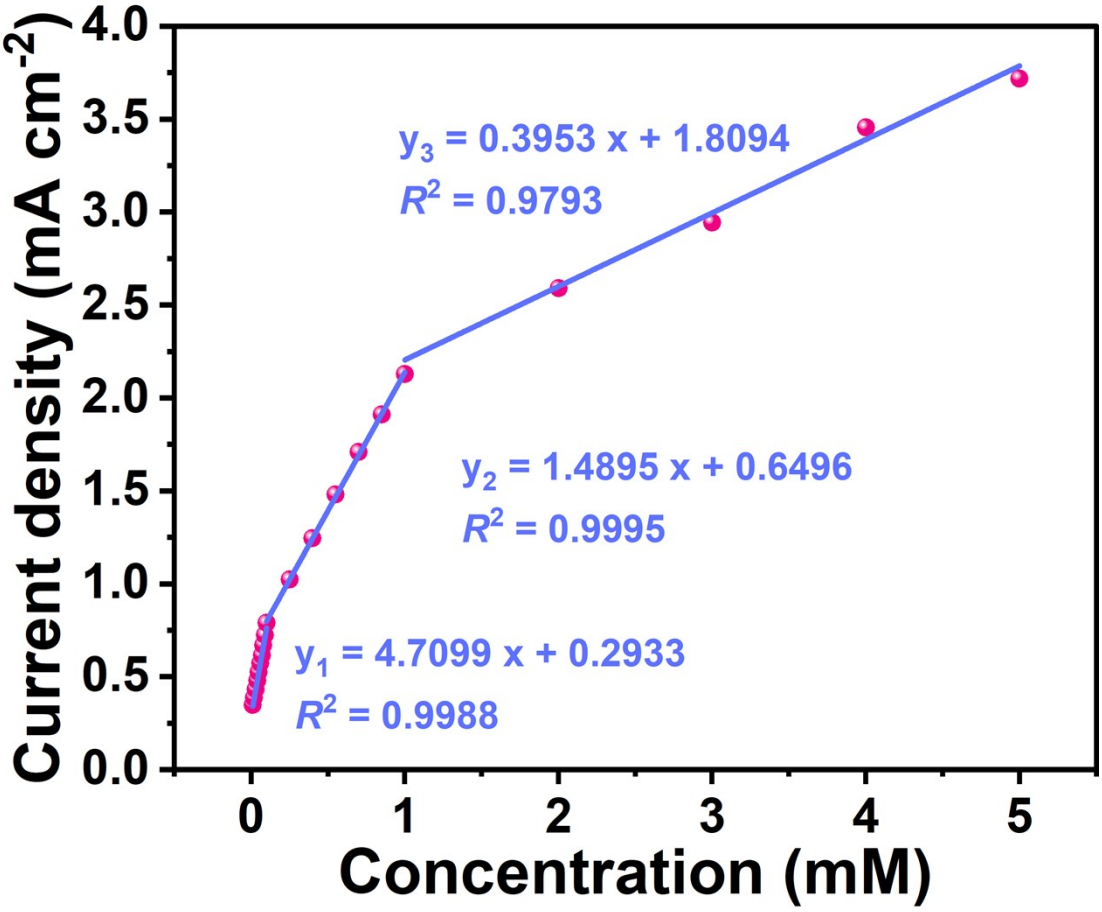

Figure S20. Three-stages linear calibration curves of CTGU-37-F.

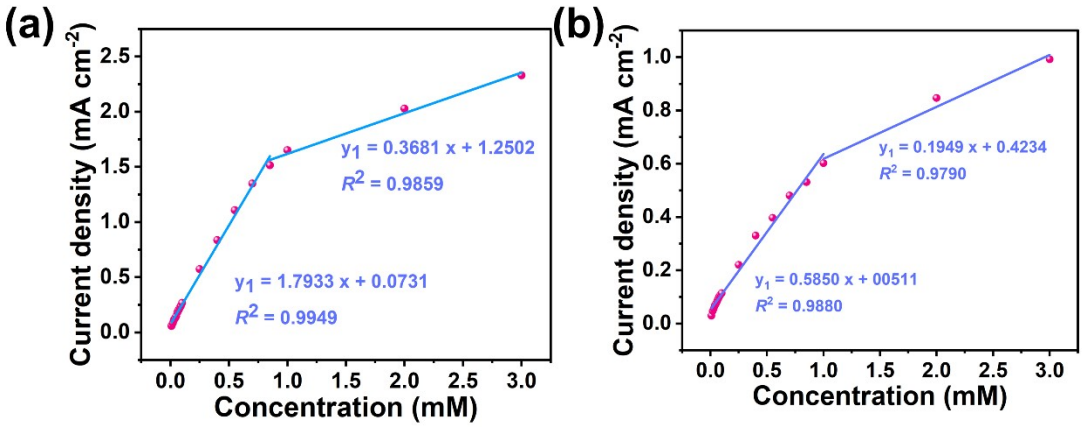

Figure S21. Corresponding linear calibration curves of (c) CTGU-37-Cl and (d) CTGU-37-Br.

Table S4. Comparisons of electrochemical glucose sensing performance

Sensors	Sensitivity ($\mu A\ mM^{-1}\ cm^{-2}$)	Limit of Detection (μM)	Linear Range (mM)	Response Time (s)	pH	Electrode Materials	Ref.
$Ni(OH)_2$ NCs/NF	7413	0.1	1-3.45	3	13	Nickel foam	[4]
NiVP/Pi	6040	0.0037	0.0001-10	/	13	Whatman filter paper	[5]
Ag-CuT/f-ES	4610	1.1	0.003-3.3	2	13	Copper tape	[6]
Ni_2Co_1-BDC	3925.3	0.29	0.0005-2.899	/	13	GCE	[7]
NiCoBP-Br	1755.5144	0.0665	0.0005-6.07	2	13	GCE	[8]
Ni-Bi NPs	677	1	0.001-3.5	25	13	GCE	[9]
PdNiP-NPs	516	0.498	0.003-1.31	1	13	Metallic glass	[10]
Ni_3C/Ni nanochain	299.4	0.28	0.001-0.0065	4	13	GCE	[11]
FeOcPc-Ni/GO/ GCE	192.13	0.625	0.002-5	/	13	GCE	[12]
Au NFs@CC	63.9	5.18	0.005-4	2.3	7.4	Carbon cloth	[13]
GOD/CoPc/PBA/BP	48.66	4.69	0.5-8	/	7	Buckypaper	[14]
TiO_2 (001)/Au/GOx	16.86	0.83	0.01-3.0	2	7.4	TiO_2 films	[15]
MXene-Cu_2O ($Ti_3C_2T_x$)	2.83	11.064	0.01-30	2	13	GCE	[16]
CTGU-37-F	4709.9	0.043	0.01-5.0	0.9	13	GCE	*This*

CTGU-37-Cl	1793.3	0.11	0.01-3.0	1.4	13		*work*
CTGU-37-Br	585.0	0.35	0.01-5.0	1.5	13		

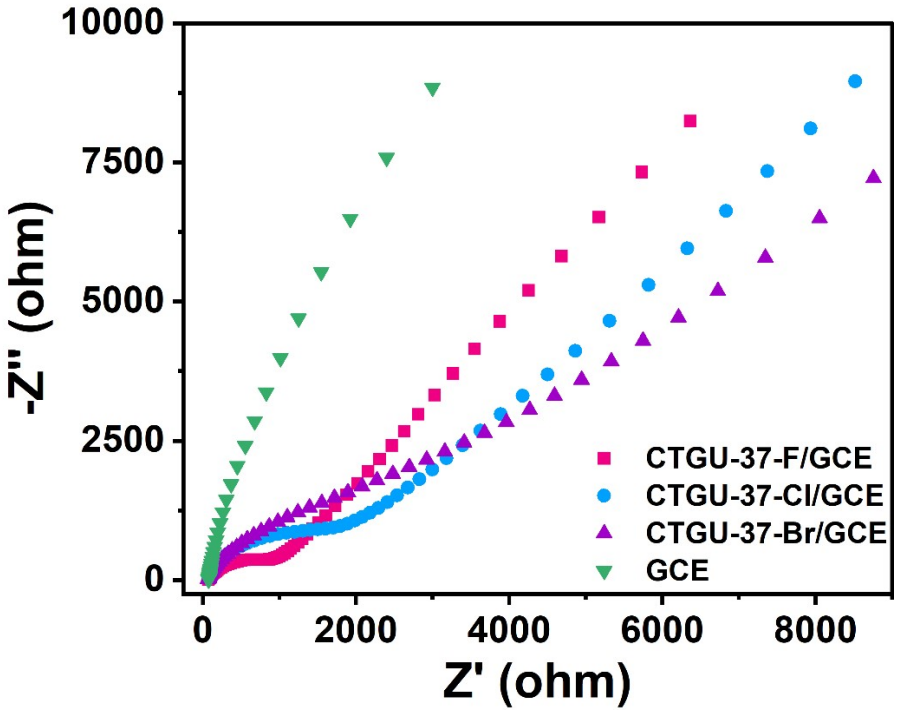

Figure S22. EIS Nyquist plots of CTGU-37-F, -Cl, -Br and bare GCE.

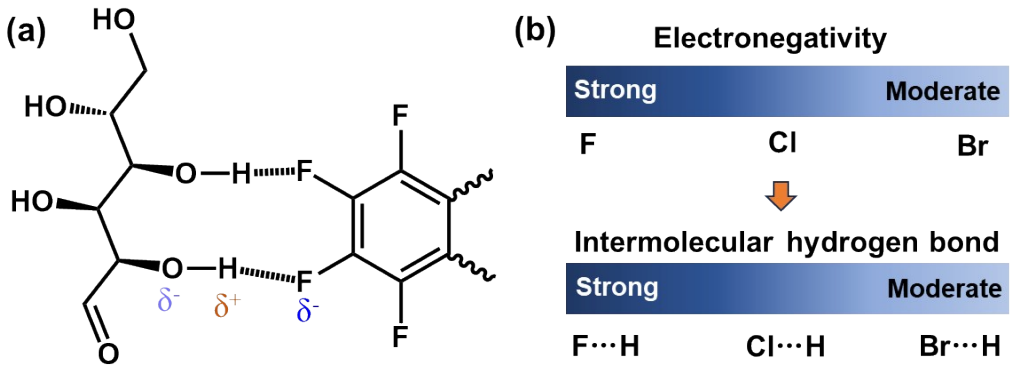

Figure S23. (a) Schematic of the intermolecular hydrogen bond between MOF and glucose. (b) Schematic of electronegativity manipulation and hydrogen bond intensity.

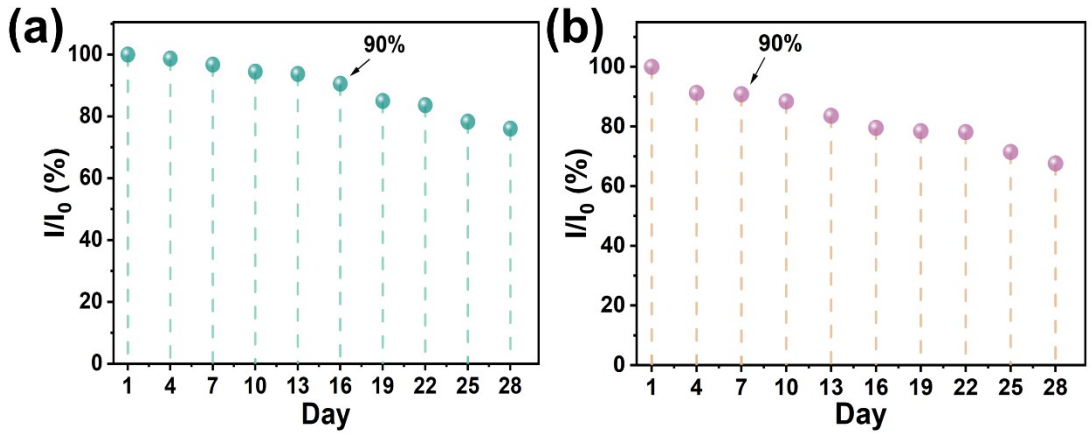

Figure S24. Percentage decrease of oxidation peak currents for each three-day interval of (c) CTGU-37-Cl and (d) CTGU-37-Br.

References

1 B. Delley, J. Chem. Phys. 1990, **92** , 508-517.

2 B. Delley, J. Chem. Phys. 2000, **113**, 7756-7764.

3 J. P. Perdew, K. Burke, M. Ernzerhof, Phys. Rev. Lett. 1996, **77**, 3865-3868.

4 F. Gao, Y. Yang, W. Qiu, Z. Song, Q. Wang and N. Li, *ACS Appl. Nano Mater*., 2021, **4**, 8520-8529.

5 B. N. Safadi, J. M. Goncalves, E. Castaldelli, T. A. Matias, P. O. Rossini, M. Nakamura, L. Angnes and K. Araki, *ChemElectroChem*., 2020, **7**, 2553-2563.

6 S.Hao, H. Zhang, X. Sun, J. Zhai, S. Dong, *Nano Res.*, 2020, **14**, 707-714.

7 W. Zheng, Y. Li and L. Y. S. Lee, *Sens. Actuators B Chem.*, 2022, **357**, 131334.

8 Y. Lou, Z. Yao, S. Fu, S. Liu, X. Zhu, W. Huang, M. Dong, J. Zeng, H. Lin, H. Zhu and S. Lan, *Prog. Nat. Sci. Mater. Int.*, 2023, **33**, 244-249.

9 A. Khoshroo, K. Sadrjavadi, M. Taran and A. Fattahi, *Sens. Actuators B Chem.,* 2020, **325**, 128778.

10 Z. Zhao, T. Wang, K. Li, D. Long, J. Zhao, F. Zhu and W. Gong, Sens. Actuators B Chem., 2023, **388**, 133798.

11 Q. Wang, Q. Jia, P. Hu and L. Ji, *Molecules*., 2023, **28**, 5469.

12 N. Thakur, D. Mandal and T. C. Nagaiah, *J. Mater. Chem. B*., 2021, **9**, 8399-8405.

13 T. S. Gopal, S. K. Jeong, T. A. Alrebdi, S. Pandiaraj, A. Alodhayb, M. Muthuramamoorthy and A. N. Grace, *Mater. Today Chem*., 2022, **24**, 100891.

14 F. Xu, K. Hu, S. Wang, X. Chen, R. Xu, X. Xiong, X. Yuan, M. Zhang and K. Huang, *J. Mater. Sci*., 2022, 57, 18589-18600.

15 W. Yang, W. Xu, Y. Wang, D. Chen, X. Wang, Y. Cao, Q. Wu, J. Tu and C. Zhen, *ACS Appl. Energy Mater.*, 2020, **3**, 2723-2732.

16 P. Li, Y. Bai, G. Zhang, X. Guo, X. Meng and H. Pang, *Inorg. Chem. Front*., 2022, 9, 5853-5861.